Polymer Journal (2017) 49, 729–734

www.nature.com/pj

ORIGINAL ARTICLE

π-conjugated naphthodithiophene homopolymers bearing alkyl/alkylthio-thienyl substituents: facile synthesis using hexamethylditin and their charge-transport and photovoltaic properties

Hideaki Komiyama[1,2], Tatsuya Oyama[1,3], Tatsuya Mori[1,3] and Takuma Yasuda[1,3]

Two π-conjugated naphtho[1,2-*b*:5,6-*b'*]dithiophene (NDT)-based homopolymers functionalized with alkyl-thienyl or alkylthio-thienyl side chains were designed and synthesized via palladium-catalyzed dehalogenative polycondensation using hexamethylditin as the condensation reagent. Their photophysical properties and device performances for organic field-effect transistors and organic solar cells were systematically studied. Replacing lateral alkyl-thienyl substituents with alkylthio-thienyl ones led to better photoabsorption properties and a deeper-lying HOMO energy level of the resulting NDT homopolymers. The alkylthio-thienyl-functionalized NDT homopolymer showed a higher hole mobility and superior photovoltaic properties compared with the alkyl-thienyl homolog.
Polymer Journal (2017) **49,** 729–734; doi:10.1038/pj.2017.45; published online 9 August 2017

INTRODUCTION

π-Conjugated polymers have attracted great interest as semiconductor materials in the field of organic electronics owing to their potential for the development of various flexible electronic devices. Organic field-effect transistors (OFETs)[1,2] and organic solar cells (OSCs)[3,4] based on these semiconducting polymers can be fabricated using printing technologies by virtue of their solution processability and superior mechanical properties. In the last decade, the performance of such organic electronic devices has rapidly improved, accompanied by the development of high-performance p-type semiconducting polymers,[5–11] including alternating electron-donor–acceptor (D–A) copolymers and electron-donor homopolymers. Currently, π-extended thienoacene derivatives, particularly benzo[1,2-*b*:4,5-*b'*]dithiophene (BDT)[12–16] and naphtho[1,2-*b*:5,6-*b'*]dithiophene (NDT),[17–24] are regarded as important building units for the design of high-performance semiconducting polymers because of their high degree of backbone coplanarity, deep-lying highest occupied molecular orbital (HOMO) energy levels, and strong intermolecular interactions. While D–A copolymers combining various electron-donor and acceptor subunits have been extensively studied, only a limited number of electron-donor homopolymers consisting of such thienoacene units have been reported thus far, in spite of their simple structures. Recently, it was reported that BDT-based homopolymers exhibited high carrier-transport properties in OFETs and high photovoltaic properties in bulk heterojunction (BHJ) OSCs.[25–30] However, there have been no precedents of NDT-based homopolymers, even though NDT derivatives have been widely used as promising electron-donor units in various D–A copolymers.[17–20]

In this work, we designed and synthesized new π-conjugated NDT-based homopolymers bearing alkylthio-thienyl or alkyl-thienyl side chains; PNDTS and PNDT (Scheme 1). The alkylthio-thienyl functionalization can stabilize the HOMO energy level of the resulting homopolymers, compared with alkyl-thienyl functionalization, which is beneficial for better air stability and higher open-circuit voltage (V_{oc}) of BHJ OSCs. Herein, we disclose the synthesis and optical, charge-transport, and photovoltaic properties of PNDTS and PNDT.

EXPERIMENTAL PROCEDURE

Synthesis of polymers

PNDTS. To a stirred solution of Br–NDTS–Br (0.27 g, 0.31 mmol) and hexamethyldithin (0.11 g, 0.33 mmol) in a mixture of dry toluene (2 ml) and dry DMF (0.5 ml) was added $Pd(PPh_3)_4$ (7.2 mg, 6.2 μmol) at 120 °C. After stirring for 24 h, 2-(tributylstannyl)thiophene (0.47 g, 1.24 mmol) was added to the mixture. The reaction mixture was further stirred for 3 h at 120 °C. After cooling to room temperature, the reaction mixture was poured into methanol. The precipitate was filtered and subjected to Soxhlet extraction with methanol, acetone, hexane, and finally chloroform. The chloroform fraction was concentrated and reprecipitated into methanol. The precipitate was collected by filtration and dried under vacuum to afford PNDTS as a dark red solid (yield = 0.17 g, 78%). GPC (eluent: THF): $M_n = 3.9$ kg mol^{-1}, $M_w = 8.3$ kg mol^{-1}, PDI = 2.1. Anal calcd (%) for $C_{38}H_{44}S_6$: C 65.85, H 6.40, S 27.75; found: C 65.10, H 5.96, S 27.43, Br 0.13.

[1]INAMORI Frontier Research Center (IFRC), Kyushu University, Fukuoka, Japan; [2]International Institute for Carbon Neutral Energy Research (WPI-I2CNER), Kyushu University, Fukuoka, Japan and [3]Department of Applied Chemistry, Graduate School of Engineering, Kyushu University, Fukuoka, Japan
Correspondence: Dr H Komiyama or Professor T Yasuda, INAMORI Frontier Research Center (IFRC), Kyushu University, 744 Motooka, Nishi-ku, Fukuoka 819-0395, Japan.
E-mail: komiyama@ifrc.kyushu-u.ac.jp or yasuda@ifrc.kyushu-u.ac.jp
Received 23 May 2017; revised 3 July 2017; accepted 5 July 2017; published online 9 August 2017

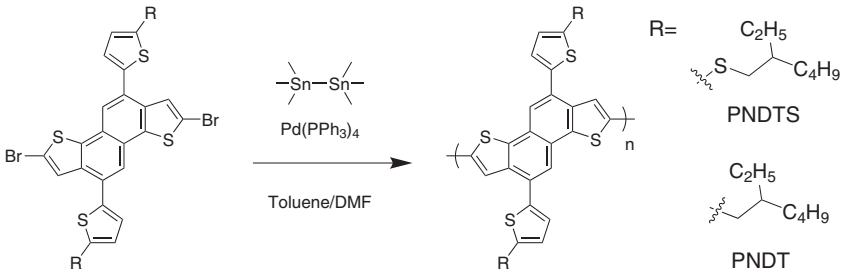

Scheme 1 Synthesis of NDT-based homopolymers.

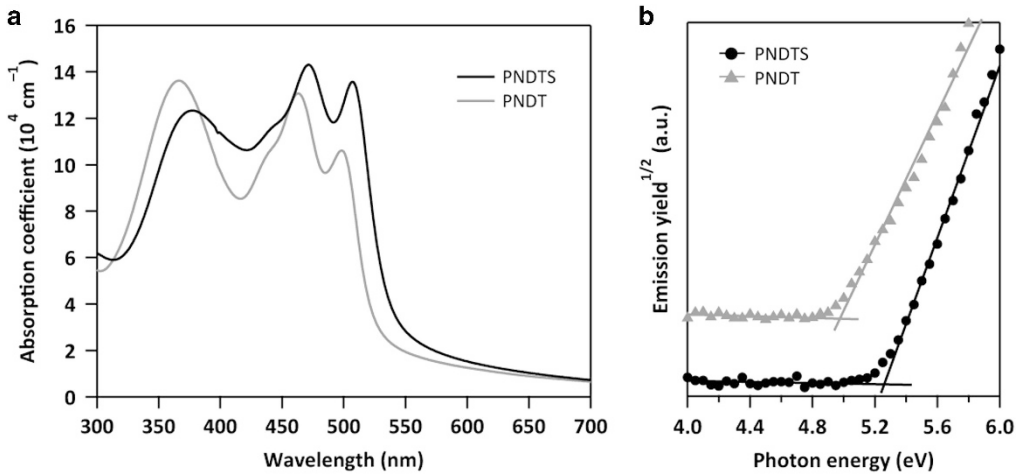

Figure 1 (**a**) UV–vis absorption spectra and (**b**) photoelectron yield spectra of PNDTS and PNDT in as-spun thin films.

PNTD. This polymer was prepared by a method similar to that of PNDTS, using Br–NDT–Br (0.31 g, 0.39 mmol), hexamethyldithin (0.14 g, 0.41 mmol), and $Pd(PPh_3)_4$ (9.0 mg, 7.8 μmol). PNDT was obtained as a dark red solid (yield = 0.21 g, 85%). GPC (eluent: THF): $M_n = 6.8$ kg mol^{-1}, $M_w = 11.7$ kg/mol, PDI = 1.7. Anal calcd (%) for $C_{38}H_{44}S_4$: C 72.56, H 7.05, S 20.39; found: C 70.30, H 6.61, S 19.32, Br 0.15.

OFET device fabrication and measurements

PNDTS and PNDT were employed for OFETs with a bottom-gate/top-contact geometry. Heavily doped *n*-type Si wafers with a thermally grown 300-nm-thick SiO_2 layer were used as the substrates. The SiO_2/Si substrates were pretreated with a piranha solution at 100 °C for 1 h, and the copiously cleaned by sonication in deionized water, acetone, and isopropanol. A self-assembled monolayer of *n*-octyltrichlorosilane was then deposited onto the SiO_2/Si substrates as an additional dielectric to reduce charge trapping by the silanol groups on SiO_2 in the devices. The polymer layer was then prepared by spin-coating from a chlorobenzene solution, after passing through a 0.45 μm PTFE membrane filter. The devices were completed by evaporating gold (thickness = 50 nm) through a shadow mask to define the source and drain electrodes with a channel length of 50–100 μm. The output and transfer characteristics of the OFETs were measured using an Agilent B1500A semiconductor parameter analyzer (Agilent Technologies, Santa Clara, CA, USA) under ambient conditions. Field-effect mobilities (μ) of OFETs were calculated in the saturation regime using the flowing equation: $I_D = (W/2L)\mu C_i (V_G - V_{th})^2$, where I_D is the source-drain current, W and L are the channel width and length, respectively, C_i is the capacitance per unit area of the gate dielectric (11.1 nF cm^{-2}), V_G is the gate voltage, and V_{th} is the threshold voltage.

OSC device fabrication and measurements

Pre-patterned ITO-coated glass substrates were cleansed sequentially by sonicating in detergent solution, deionized water, acetone, and isopropanol for 15 min each, and then subjected to UV/ozone treatment for 30 min. A thin layer (~30 nm) of ZnO was prepared by spin-coating (at 5000 r.p.m.) a precursor solution of zinc acetate dehydrate (0.50 g) and ethanolamine (0.14 g) in 2-methoxyethanol (5 ml), followed by baking at 200 °C for 10 min under air. The photoactive layer was then prepared by spin-coating from a chlorobenzene solution containing the polymer and [6,6]-phenyl-C_{71}-butyric acid methylester ($PC_{71}BM$), after passing through a 0.45 μm PTFE membrane filter. Finally, a 10-nm-thick MoO_3 layer and a 100-nm-thick Ag layer were thermally evaporated on top of the active layer under high vacuum through a shadow mask, defining an active area of 0.04 cm^2 for each device. Current density–voltage (*J*–*V*) and incident photon-to-current conversion efficiency (IPCE) measurements for the fabricated OSCs were conducted on a computer-controlled Keithley 2400 source measure unit in air, under simulated AM 1.5G solar illumination at 100 mW cm^{-2} (1 sun), using a Xe lamp-based Bunko-Keiki SRO-25 GD solar simulator and IPCE measurement system (Bunko-Keiki, Tokyo, Japan). The light intensity was calibrated using a standard silicon photovoltaic reference cell.

RESULTS AND DISCUSSION

Synthesis and characterization

For the synthesis of NDT-based homopolymers, we performed the dehalogenative polycondensation of the corresponding dibromo monomers [Br-NDT(S)-Br] using hexamethylditin as the condensation reagent[31] in the presence of a catalytic amount of $Pd(PPh_3)_4$ (Scheme 1). The detailed synthetic processes for the dibromo monomers are described in Supplementary Information. The resulting polymers were purified by reprecipitation, followed by Soxhlet extractions with methanol, acetone, and hexane. The weight-average molecular weights (M_w) and polydispersity indices (PDI) of the THF soluble parts were $M_w = 8.3$ kg mol^{-1} and PDI = 2.1 for PNDTS and $M_w = 11.7$ kg mol^{-1} and PDI = 1.7 for PNDT, as determined by gel permeation chromatography analysis using a polystyrene standard in a

THF eluent. The M_w values might be underestimated due to lower solubility of these polymers in THF. The end-capping of the polymers with thiophene was confirmed by elemental analysis for Br contents. These polymers showed enough high solubility in chlorobenzene and *o*-dichlorobenzene at room temperature, which ensured the OFET and OSC device fabrications. Thermogravimetric analysis of PNDTS and PNDT indicated 5% weight-loss temperatures (T_d) of 326 and 314 °C, respectively, under N_2 (Supplementary Figure S1). The present polycondensation method utilizing hexamethylditin is useful for the synthesis of these thienoacene-based homopolymers because the corresponding dibromo monomers can be used directly for the polymerization reactions without preparing any unstable organometallic intermediates. The widely used straightforward method for producing these π-conjugated homopolymers is polycondensation via Stille cross-coupling reactions using both distannyl and dibromo monomers, which requires two different monomers to be prepared independently.[27–29]

Table 1 Summary of photophysical properties of PNDTS and PNDT

	solution[a]	*thin film*[b]				
polymer	λ_{max} *(nm)*	λ_{max} *(nm)*	α *(cm^{-1})*	*HOMO (eV)*[c]	*LUMO (eV)*[d]	E_g *(eV)*[e]
PNDTS	371, 467, 501	375, 471, 507	14.3×10^4	−5.25	−2.96	2.29
PNDT	364, 454, 480	366, 463, 498	13.1×10^4	−4.97	−2.62	2.35

[a]In chloroform solution (0.01 g l^{-1}).
[b]Spin-coated from chlorobenzene solution onto quartz substrates.
[c]Determined by photoelectron yield spectroscopy in thin films.
[d]Determined according to the HOMO and optical energy gap (E_g) using LUMO = HOMO+E_g.
[e]Derived from the absorption onset of the thin films.

Optical properties

UV–vis absorption spectra of PNDTS and PNDT in as-spun thin films are shown in Figure 1a. The relevant photophysical data are summarized in Table 1. These polymers exhibited three characteristic absorption bands. The absorption spectra in chloroform solutions are similar to those in the solid thin films (Supplementary Figure S2), implying the formation of aggregates even in the solution state. The absorption peaks of PNDTS in the thin film are slightly red-shifted compared to that of PNDT, suggesting the extension of the effective π-conjugation length and the increment of intermolecular interactions, which were presumably due to additional thioether groups in PNDTS. The optical bandgaps (E_g) of PNDTS and PNDT were estimated to be 2.29 and 2.35 eV, respectively, according to the onset positions of their lowest-energy absorption bands in the thin films. From the photoelectron yield spectroscopy (Figure 1b), the HOMO energy levels of PNDTS and PNDT were determined to be −5.25 and −4.97 eV, respectively, indicative of the deeper-lying HOMO energy level of PNDTS. The lowest unoccupied molecular orbital (LUMO) energy levels of PNDTS and PNDT (−2.96 and −2.62 eV, respectively) were sufficiently higher than that of [6,6]-phenyl-C_{71}-butyric acid methylester ($PC_{71}BM$; LUMO = −4.3 eV) to enable directed photoinduced charge transfer. Accordingly, both PNDTS and PNDT can be utilized

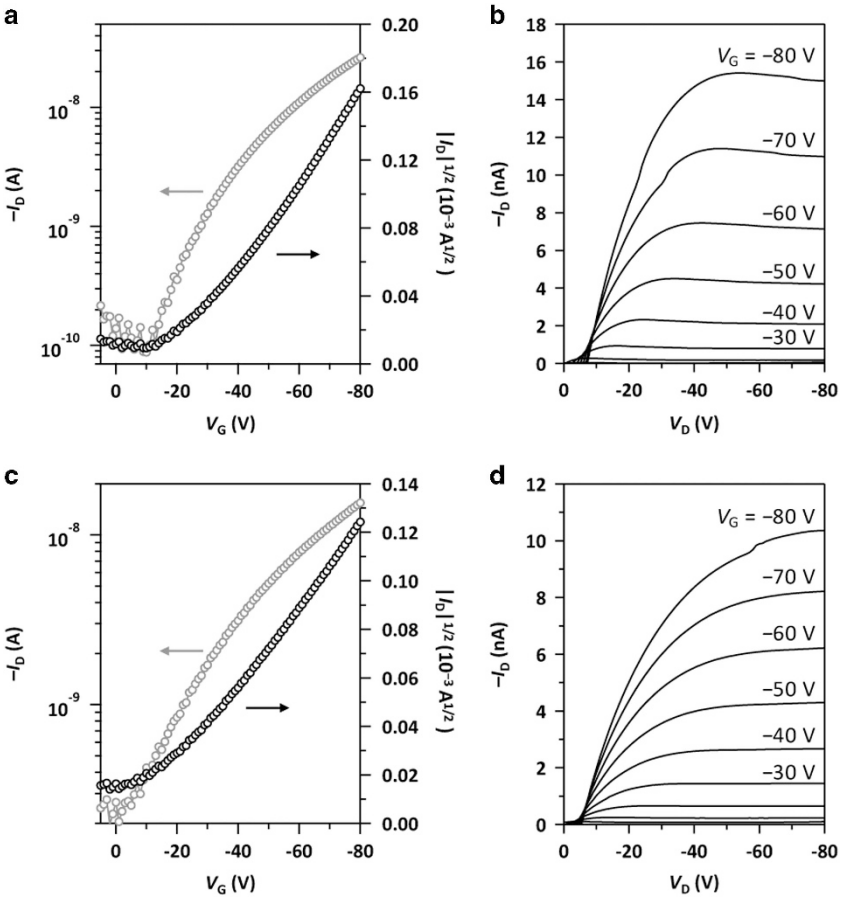

Figure 2 Charge–carrier transport properties: (left) output characteristics at $V_D = -80$ V and (right) transfer characteristics of OFETs based on (**a**, **b**) PNDTS and (**c**, **d**) PNDT with channel width/length of 1000/100 μm and 1000/60 μm, respectively.

Table 2 Summary of device performances of PNDTS and PNDT

	OFET[a]			*OSC*[b]				
polymer	μ ($cm^2\ V^{-1}\ s^{-1}$)	I_{on}/I_{off}	V_{th} (V)	*Thickness (nm)*	J_{sc} ($mA\ cm^{-2}$)	V_{oc} (V)	*FF (%)*	*PCE (%)*
PNDTS	1.4×10^{-4} ($(1.4\pm0.2)\times10^{-4}$)	$\sim10^3$	−24	69	7.83	0.84	45	3.0 (2.9±0.1)
PNDT	3.8×10^{-5} ($(3.5\pm0.3)\times10^{-5}$)	$\sim10^2$	−10	62	7.22	0.78	44	2.5 (2.4±0.1)

[a]OFET characteristics of the polymers measured using a device structure of a top-contact/bottom-gate geometry with Au electrodes; μ: hole mobility; V_{th}: threshold voltage determined by the $I_D^{1/2}$ vs V_G plot; I_{on}/I_{off}: on/off current ratio determined according to I_D at $V_G=0$ V (I_{off}) and $V_G=80$ V (I_{on}); the values in parentheses are averaged μ values obtained from individual four devices.
[b]OSC characteristics measured using a device structure of ITO/ZnO/polymer:$PC_{71}BM$ (1:1, w/w)/MoO_3/Ag with the active area of 0.04 cm^2, under AM 1.5G (100 mW cm^{-2}); the values in parentheses are averaged PCE values obtained from individual four devices.

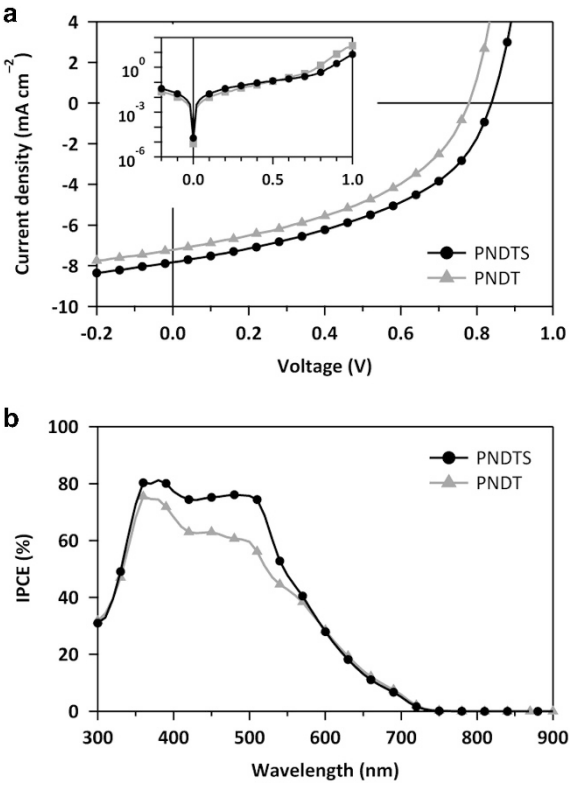

Figure 3 Photovoltaic properties of the polymers: (**a**) *J–V* curves (inset: dark *J–V* curves) and (**b**) IPCE spectra for BHJ OSCs based on PNDTS:$PC_{71}BM$ (1:1, w/w) and PNDT:$PC_{71}BM$ (1:1, w/w), measured under AM 1.5G (100 mW cm^{-2}).

as donor materials in OSC devices with $PC_{71}BM$ as an acceptor material, as discussed later.

We also performed density functional theory calculations for the corresponding pentamers as models of PNDTS and PNDT at the B3LYP/6-31(d) level (Supplementary Figure S3). The distributions of the HOMO and LUMO wave functions in both molecules appeared to be very similar and were delocalized over their π-conjugated backbone. More importantly, replacing alkyl groups with thioalkyl groups indeed deepened the HOMO energy level because of the reduced electron-donating ability of the thioalkyl groups.[32–34]

Charge-transport properties

To evaluate the charge-transport properties, top-contact/bottom-gate OFETs based on PNDTS and PNDT were fabricated by spin-coating their chlorobenzene solutions onto *n*-octyltrichlorosilane-treated SiO_2/Si substrates, followed by the vacuum-deposition of Au source and drain electrodes. The output and transfer characteristics of the PNDTS- and PNDT-based OFETs are shown in Figure 2, and the hole mobilities (μ) calculated according to the saturated regime, current on/off ratios (I_{on}/I_{off}), and threshold voltages (V_{th}) are listed in Table 2. Both OFET devices exhibited typical p-type transistor behavior under ambient conditions. The hole mobility of PNDTS ($\mu=1.4\times10^{-4}\ cm^2\ V^{-1}\ s^{-1}$) was substantially higher than that of PNDT ($\mu=3.8\times10^{-5}\ cm^2\ V^{-1}\ s^{-1}$). Grazing incidence wide-angle X-ray scattering (GIWAXS) measurements revealed that PNDTS had a stronger tendency to take an edge-on orientation on the substrate than PNDT (Supplementary Figure S4 and Supplementary Table S1). Thus, better charge-carrier transport along the parallel direction to the substrate was attained with PNDTS through π–π interactions in OFETs. The V_{th} value is generally proportional to the energy difference between the electrode work function and the HOMO level of the incorporated p-type semiconductor. PNDTS, with a deeper HOMO level of −5.25 eV, indeed required a negatively large gate bias ($V_{th}=-24$ V) to accumulate holes at the dielectric interface compared with PNDT ($V_{th}=-10$ V), which had a shallower HOMO level of −4.97 eV.

Photovoltaic properties

BHJ OSCs were fabricated by spin-coating polymer/$PC_{71}BM$ blend solutions in chlorobenzene onto a ZnO-deposited ITO glass substrate, followed by the vacuum-deposition of MoO_3 as a hole-extraction layer and Ag as an anode.[35] The OSCs were optimized by changing the weight ratio of the polymer/$PC_{71}BM$ BHJ blends to 1:2, 1:1, and 2:1 (Supplementary Figure S5 and Supplementary Table S2), and both the PNDTS- and PNDT-based devices exhibited the best performance with the weight ratio of 1:1. Figure 3a shows the current density–voltage (*J–V*) characteristics of PNDTS- and PNDT-based BHJ OSCs with the optimal weight ratio, measured under simulated AM 1.5G illumination (100 mW cm^{-2}). The key photovoltaic parameters are listed in Table 2. The PNDTS-based OSC showed a higher power-conversion efficiency (PCE) of 3.0% with an open-circuit voltage (V_{oc}) of 0.84 V, a short-circuit current density (J_{sc}) of 7.83 mA cm^{-2}, and a fill factor (FF) of 45%, while the PNDT-based OSC had a PCE of 2.5% with a V_{oc} of 0.78 V, a J_{sc} of 7.22 mA cm^{-2}, and a FF of 44%.

The incident photon-to-current conversion efficiency (IPCE) spectra of the optimal BHJ OSCs indicate intense photocurrent responses in the range of 350–550 nm (Figure 3b), which agrees well with the optical absorption of these polymers (Figure 1a). It should be noted that PNDTS with a deeper HOMO energy level exhibited a lager V_{oc} of up to 0.90 V than that of PNDT. In general, the V_{oc} of BHJ OSCs is closely correlated with the energy difference between the HOMO of the donor material and the LUMO of the acceptor material ($PC_{71}BM$).[36] Therefore, the introduction of alkylthio-thienyl substituents in PNDTS increased the V_{oc} of the photovoltaic device.

To characterize the microstructures and molecular orientations in the solid states, GIWAXS measurements were performed for the

polymer/$PC_{71}BM$ (1:1, w/w) BHJ blend films. The two-dimensional (2D) GIWAXS images of the blend films are shown in Figure 4a, and their line cut profiles for the out-of-plane (q_z) and in-plane (q_{xy}) directions are shown in Figure 4b, c respectively (see Supplementary Table S3 for detailed packing parameters). Both the PNDTS- and PNDT-based blend films showed a semi-crystalline nature and a preferred edge-on orientation on substrates with the lamellar spacings (d_{100}) of 25.0 and 22.8 Å, respectively, suggesting that the incorporation of alkylthio-thienyl substituents in PNDTS slightly increased the lamellar spacing. The π–π stacking distance (d_{010}) for PNDTS and PNDT was observed at 3.5 Å, which is comparable to that of BDT-based homopolymer[28] but smaller than those of conventional thiophene-based polymers such as P3HT.[37] Thus, PNDTS and PNDT appear to form relatively tight interchain packing in the BHJ blend films, owing to the high coplanarity of NDT units.

CONCLUSIONS

In conclusion, two novel π-conjugated NDT-based homopolymers, PNDTS and PNDT, were designed and synthesized. To simplify the synthesis route, we employed palladium-catalyzed dehalogenative polycondensation with hexamethylditin as the condensation reagent. Replacing alkyl-thienyl groups with alkylthio-thienyl groups resulted in the deepening of the HOMO energy level of the resulting polymers, which was beneficial for photovoltaic applications. OFET and BHJ OSC devices based on PNDTS exhibited a higher hole mobility and PCE than PNDT-based devices. Moreover, PNDTS-based BHJ OSCs showed a large V_{oc} up to 0.90 V because the alkylthio-thienyl groups lowered the HOMO energy level of the polymer, which makes PNDTS a promising donor material for BHJ OSCs.

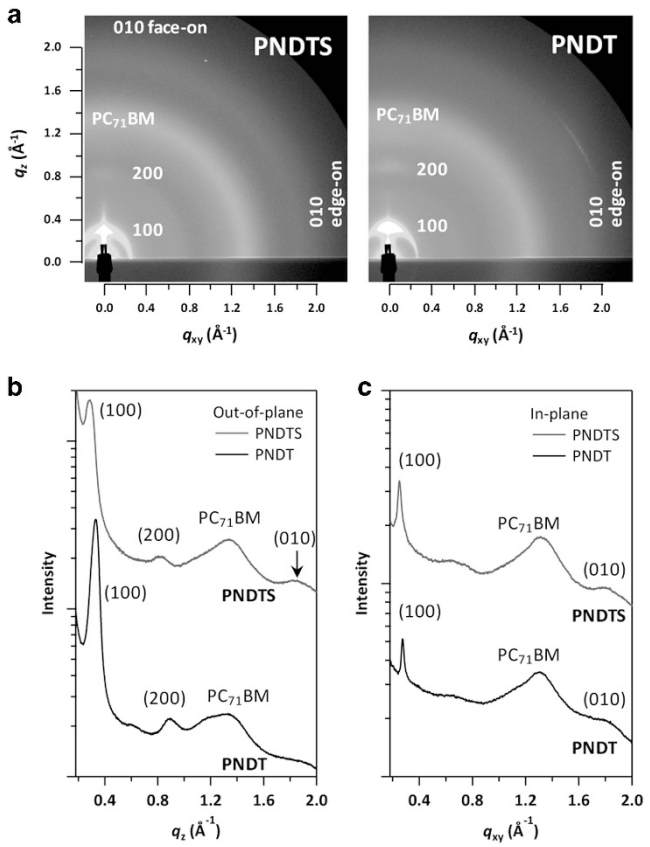

Figure 4 (**a**) 2D GIWAXS patterns of blend films of PNDTS and PNDT with $PC_{71}BM$ (1:1, w/w). (**b**) Out-of-plane (q_z-scan) and (**c**) in-plane (q_{xy}-scan) profiles of the corresponding blend films.

CONFLICT OF INTEREST

The authors declare no conflict of interest.

ACKNOWLEDGEMENTS

This work was partially supported by Grants-in-Aid for Scientific Research (Nos. 16K21218 (HK) and 15H01049 (TY)) from JSPS, the Cooperative Research Program of 'Network Joint Research Center for Materials and Devices', the Yoshida Education and Foundation, the Izumi Science and Technology Foundation, the ATI Research Grants 2016 (HK), the KDDI Foundation, and the Canon Foundation (TY). The GIWAXS measurements were performed at the BL40-B2 of SPring-8 with the approval of the Japan Synchrotron Radiation Research Institute (JASRI) (Proposal No. 2016B1118). HK acknowledge the support of WPI-I2CNER, sponsored by MEXT, Japan.

1 Yan, H., Chen, Z., Zheng, Y., Newman, C., Quinn, J. R., Dötz, F., Kastler, M. & Facchetti, A. A high-mobility electron-transporting polymer for printed transistors. *Nature* **457**, 679–686 (2009).
2 Holliday, S., Donaghey, J. E. & McCulloch, I. Advances in charge carrier mobilities of semiconducting polymers used in organic transistors. *Chem. Mater.* **26**, 647–663 (2014).
3 Zhou, H., Yang, L. & You, W. Rational design of high performance conjugated polymers for organic solar cells. *Macromolecules* **45**, 607–632 (2012).
4 Kang, H., Kim, G., Kim, J., Kwon, S., Kim, H. & Lee, K. Bulk-heterojunction organic solar cells: five core technologies for their commercialization. *Adv. Mater.* **28**, 7821–7861 (2016).
5 Beaujuge, P. M. & Frechet, J. M. Molecular design and ordering effects in π-functional materials for transistor and solar cell applications. *J. Am. Chem. Soc.* **133**, 20009–20029 (2011).
6 Li, J., Zhao, Y., Tan, H. S., Guo, Y., Di, C. A., Yu, G., Liu, Y., Lin, M., Lim, M. S. H., Zhou, Y., Su, H. & Ong, B. S. A stable solution-processed polymer semiconductor with record high-mobility for printed transistors. *Sci. Rep.* **2**, 754 (2012).
7 Kawashima, K., Fukuhara, T., Suda, Y., Suzuki, Y., Koganezawa, T., Yoshida, H., Ohkita, H., Osaka, I. & Takimiya, K. Implication of fluorine atom on electronic properties, ordering structures, and photovoltaic performance in naphthobisthiadiazole-based semiconducting polymers. *J. Am. Chem. Soc.* **138**, 10265–10275 (2016).
8 Fukuta, S., Wang, Z., Miyane, S., Koganezawa, T., Sano, T., Kido, J., Mori, H., Ueda, M. & Higashihara, T. Synthesis of 1,3,4-thiadiazole-based donor–acceptor alternating copolymers for polymer solar cells with high open-circuit voltage. *Polym. J.* **47**, 513–521 (2015).
9 Nakashima, M., Otsura, T., Naito, H. & Ohshita, J. Synthesis of new D–A polymers containing disilanobithiophene donor and application to bulk heterojunction polymer solar cells. *Polym. J.* **47**, 733–738 (2015).
10 Nguyen, Y. L., Choi, H., Ko, J. K., Kim, T., Uddin, M. A., Jin, S. H., Kim, Y. & Woo, H. Y. Semi-crystalline A_1–D–A_2-type copolymers for efficient polymer solar cells. *Polym. J.* **49**, 141–148 (2017).
11 Kawabata, K., Saito, M., Takemura, N., Osaka, I. & Takimiya, K. Effects of branching position of alkyl side chains on ordering structure and charge transport property in thienothiophenedione- and quinacridone-based semiconducting polymers. *Polym. J.* **49**, 169–176 (2017).
12 Yuan, J., Huang, X., Zhang, F., Lu, J., Zhai, Z., Di, C., Jiang, Z. & Ma, W. Design of benzodithiophene-diketopyrrolopyrrole based donor–acceptor copolymers for efficient organic field effect transistors and polymer solar cells. *J. Mater. Chem.* **22**, 22734–22742 (2012).
13 Ko, S., Kim, D. H., Ayzner, A. L., Mannsfeld, S. C. B., Verploegen, E., Nardes, A. M., Kopidakis, N., Toney, M. F. & Bao, Z. Thermotropic phase transition of benzodithiophene copolymer thin films and its impact on electrical and photovoltaic characteristics. *Chem. Mater.* **27**, 1223–1232 (2015).
14 Liang, Y., Xu, Z., Xia, J., Tsai, S. T., Wu, Y., Li, G., Ray, C. & Yu, L. For the bright future-bulk heterojunction polymer solar cells with power conversion efficiency of 7.4%. *Adv. Mater.* **22**, E135–E138 (2010).
15 Liao, S. H., Jhuo, H. J., Cheng, Y. S. & Chen, S. A. Fullerene derivative-doped zinc oxide nanofilm as the cathode of inverted polymer solar cells with low-bandgap polymer (PTB7-Th) for high performance. *Adv. Mater.* **25**, 4766–4771 (2013).
16 Nakabayashi, K., Otani, H. & Mori, H. Benzodithiophene-based low band-gap polymers with deep HOMO levels: synthesis, characterization, and photovoltaic performance. *Polym. J.* **47**, 617–623 (2015).
17 Osaka, I., Kakara, T., Takemura, N., Koganezawa, T. & Takimiya, K. Naphthodithiophene-naphthobisthiadiazole copolymers for solar cells: alkylation drives the polymer backbone flat and promotes efficiency. *J. Am. Chem. Soc.* **135**, 8834–8837 (2013).

18 Osaka, I., Houchin, Y., Yamashita, M., Kakara, T., Takemura, N., Koganezawa, T. & Takimiya, K. Contrasting effect of alkylation on the ordering structure in isomeric naphthodithiophene-based polymers. *Macromolecules* **47**, 3502–3510 (2014).
19 Zhu, X., Fang, J., Lu, K., Zhang, J., Zhu, L., Zhao, Y., Shuai, Z. & Wei, Z. Naphtho[1,2-*b*:5,6-*b*′]dithiophene based two-dimensional conjugated polymers for highly efficient thick-film inverted polymer solar cells. *Chem. Mater.* **26**, 6947–6954 (2014).
20 Cheng, S. W., Tsai, C. E., Liang, W. W., Chen, Y. L., Cao, F. Y., Hsu, C. S. & Cheng, Y. J. Angular-shaped 4,9-dialkylnaphthodithiophene-based donor–acceptor copolymers for efficient polymer solar cells and high-mobility field-effect transistors. *Macromolecules* **48**, 2030–2038 (2015).
21 Bathula, C., Song, C. E., Badgujar, S., Hong, S. J., Park, S. Y., Shin, W. S., Lee, J. C., Cho, S., Ahn, T., Moon, S. J. & Lee, S. K. Naphtho[1,2-*b*:5,6-*b*′]dithiophene-based copolymers for applications to polymer solar cells. *Polym. Chem.* **4**, 2132–2139 (2013).
22 Shi, S., Xie, X., Jiang, P., Chen, S., Wang, L., Wang, M., Wang, H., Li, X., Yu, G. & Li, Y. Naphtho[1,2-*b*:5,6-*b*′]dithiophene-based donor–acceptor copolymer semiconductors for high-mobility field-effect transistors and efficient polymer solar cell.s. *Macromolecules* **46**, 3358–3366 (2013).
23 Dutta, P., Park, H., Lee, W. H., Kang, I. N. & Lee, S. H. Synthesis characterization and bulk-heterojunction photovoltaic applications of new naphtho[1,2-*b*:5,6-*b*′]dithiophene–quinoxaline containing narrow band gap D–A conjugated polymers. *Polym. Chem.* **5**, 132–143 (2014).
24 Shi, S., Shi, K., Qu, R., Mao, Z., Wang, H., Yu, G., Li, X. & Li, Y. Alkylphenyl substituted naphthodithiophene: a new building unit with conjugated side chains for semiconducting materials. *Macromol. Rapid Commun.* **35**, 1886–1889 (2014).
25 Pan, H., Li, Y., Wu, Y., Liu, P., Ong, B. S., Zhu, S. & Xu, G. Synthesis and thin-film transistor performance of poly(4,8-didodecylbenzo[1,2-*b*:4,5-*b*′]dithiophene). *Chem. Mater.* **18**, 3237–3241 (2006).
26 Sista, P., Bhatt, M. P., McCary, A. R., Nguyen, H., Hao, J., Biewer, M. C. & Stefan, M. C. Enhancement of OFET performance of semiconducting polymers containing benzodithiophene upon surface treatment with organic silanes. *J. Polym. Sci. Part A: Polym. Chem.* **49**, 2292–2302 (2011).
27 Lee, D., Hubijar, E., Kalaw, G. J. D. & Ferraris, J. P. Enhanced and tunable open-circuit voltage using dialkylthio benzo[1,2-*b*:4,5-*b*′]dithiophene in polymer solar cells. *Chem. Mater.* **24**, 2534–2540 (2012).
28 Kang, T. E., Kim, T., Wang, C., Yoo, S. & Kim, B. J. Poly(benzodithiophene) homopolymer for high-performance polymer solar cells with open-circuit voltage of near 1 V: a superior candidate to substitute for poly(3-hexylthiophene) as wide bandgap polymer. *Chem. Mater.* **27**, 2653–2658 (2015).
29 Kim, J. H., Park, J. B., Yoon, S. C., Jung, I. H. & Hwang, D. H. Enhanced and controllable open-circuit voltage using 2D-conjugated benzodithiophene (BDT) homopolymers by alkylthio substitution. *J. Mater. Chem. C* **4**, 2170–2177 (2016).
30 Magurudeniya, H. D., Kularatne, R. S., Rainbolt, E. A., Bhatt, M. P., Murphy, J. W., Sheina, E. E., Gnade, B. E., Biewer, M. C. & Stefan, M. C. Benzodithiophene homopolymers synthesized by Grignard metathesis (GRIM) and Stille coupling polymerizations. *J. Mater. Chem. A* **2**, 8773–8781 (2014).
31 Yasuda, T., Sakai, Y., Aramaki, S. & Yamamoto, T. New coplanar $(ABA)_n$-type donor-acceptor π-conjugated copolymers constituted of alkylthiophene (unit A) and pyridazine (Unit B): synthesis using hexamethylditin, self-organized solid structure, and optical and electrochemical properties of the copolymers. *Chem. Mater.* **17**, 6060–6068 (2005).
32 Cui, C., Wong, W. Y. & Li, Y. Improvement of open-circuit voltage and photovoltaic properties of 2D-conjugated polymers by alkylthio substitution. *Energy Environ. Sci.* **7**, 2276–2284 (2014).
33 Min, J., Cui, C., Heumueller, T., Fladischer, S., Cheng, X., Spiecker, E., Li, Y. & Brabec, C. J. Side-chain engineering for enhancing the properties of small molecule solar cells: a trade-off beyond efficiency. *Adv. Energy Mater.* **6**, 1600515 (2016).
34 Yao, H., Zhang, H., Ye, L., Zhao, W., Zhang, S. & Hou, J. Dialkylthio substitution: an effective method to modulate the molecular energy levels of 2D-BDT photovoltaic polymers. *ACS Appl. Mater. Interfaces* **8**, 3575–3583 (2016).
35 Shin, W., Yasuda, T., Hidaka, Y., Watanabe, G., Arai, R., Nasu, K., Yamaguchi, T., Murakami, W., Makita, K. & Adachi, C. π-Extended narrow-bandgap diketopyrrolopyrrole-based oligomers for solution-processed inverted organic solar cells. *Adv. Energy Mater.* **4**, 1400879 (2014).
36 Scharber, M. C., Mühlbacher, D., Koppe, M., Denk, P., Waldauf, C., Heeger, A. J. & Brabec, C. J. Design rules for donors in bulk-heterojunction solar cells-towards 10 % energy-conversion efficiency. *Adv. Mater.* **18**, 789–794 (2006).
37 Hopkinson, P. E., Staniec, P. A., Pearson, A. J., Dunbar, A. D. F., Wang, T., Ryan, A. J., Jones, R. A. L., Lidzey, D. G. & Donald, A. M. A phase diagram of the P3HT:PCBM organic photovoltaic system: implications for device processing and performance. *Macromolecules* **44**, 2908–2917 (2011).

Supplementary Information accompanies the paper on Polymer Journal website (http://www.nature.com/pj)